Journal of
Materials Chemistry C

Impacts of Extending π-Conjugation of the 2,2′-Biquinoline Ligand on Photophysics and Reverse Saturable Absorption of the Heteroleptic Cationic Iridium(III) Complexes

Journal:	*Journal of Materials Chemistry C*
Manuscript ID	TC-ART-08-2021-003601.R1
Article Type:	Paper
Date Submitted by the Author:	09-Oct-2021
Complete List of Authors:	Lu, Taotao; North Dakota State University, Department of Chemistry and Biochemistry Lu, Cuifen; Hubei University; North Dakota State University, Department of Chemistry and Biochemistry Cui, Peng; North Dakota State University, Department of Chemistry and Biochemistry Kilina, Svetlana; North Dakota State University, Chemistry and Biochemistry Sun, Wenfang; North Dakota State University, Chemistry

ARTICLE

Impacts of Extending π-Conjugation of the 2,2′-Biquinoline Ligand on Photophysics and Reverse Saturable Absorption of the Heteroleptic Cationic Iridium(III) Complexes

Received 00th January 20xx,
Accepted 00th January 20xx

DOI: 10.1039/x0xx00000x

Taotao Lu,[a,‡] Cuifen Lu,[a,b,‡] Peng Cui,[c,a] Svetlana Kilina,[a] Wenfang Sun[a,*]

Two heteroleptic monocationic Ir(III) complexes bearing 6,6′-bis(7-benzothiazolylfluoren-2-yl)-2,2′-biquinoline as the diimine ligand with different degrees of π-conjugation were synthesized and their photophysics were investigated by spectroscopic techniques and first principle calculations. These complexes possessed two intense absorption bands at 300-380 nm and 380-520 nm in toluene that are predominantly ascribed to the diimine ligand-localized $^1\pi,\pi^*$ transition and intraligand charge transfer (^{1}ILCT)/$^1\pi,\pi^*$ transitions, respectively, with the latter being mixed with minor ^{1}MLCT (metal-to-ligand charge transfer) / ^{1}LLCT (ligand-to-ligand charge transfer) configurations. Both complexes also exhibited a spin-forbidden, very weak ^{3}MLCT/^{3}LLCT/$^3\pi,\pi^*$ absorption band at 520-650 nm. The emission of these complexes appeared in the red spectral region (λ_{em}: 640 nm for **Ir-1** and 648 nm for **Ir-2** in toluene) with a quantum yield of <10% and a lifetime of hundreds of ns, which emanated from the ^{3}ILCT/$^3\pi,\pi^*$ state. The ^{3}ILCT/$^3\pi,\pi^*$ state also gave rise to broad and moderately strong transient absorption (TA) at ca. 480-800 nm. Extending the π-conjugation of the diimine ligand via inserting C≡C triplet bonds between the 7-benzothiazolylfluoren-2-yl substituents and 2,2′-biquinoline slightly red-shifted the absorption bands, the emission bands, and the TA bands in **Ir-2** compared to those in **Ir-1** that lacks the connecting C≡C triplet bonds in the diimine ligand. The stronger excited-state absorption with respect to the ground-state absorption at 532 nm led to strong revers saturable absorption (RSA) for ns laser pulses at this wavelength, with the RSA of **Ir-2** being slightly stronger than that of **Ir-1**, which correlated well with their ratios of the excited-state to ground-state absorption cross sections (σ_{ex}/σ_0). These results suggest that extending π-conjugation of the 2,2′-biquinoline ligand *via* incorporating the 7-benzothiazolylfluoren-2-yl substituents retained the broad but weak ground-state absorption at 500-650 nm, meanwhile increased the triplet excited-state lifetimes that resulted in the much stronger triplet excited-state absorption in this spectral regions and strong RSA at 532 nm. Thus, these complexes are promising candidates as broadband reverse saturable absorbers.

Introduction

Transition-metal complexes possessing unique optical and electronic properties have attracted great interest in the past a few decades.[1] Among the variety of transition-metal complexes, iridium(III) complexes featuring d^6 transition-metal center and octahedral coordination geometry appear particularly attractive due to their intriguing photophysical and photochemical properties.[2-5] The 5d orbitals in iridium have one of the largest spin-orbit coupling constants among all transition metals, which facilitates intersystem crossing from the singlet to the triplet state. Consequently, Ir(III) complexes typically possess high triplet quantum yields and phosphorescence at room temperature. This feature holds great potential for a variety of applications, such as light-emitting electrochemical cells (LEECs),[6,7] organic light-emitting devices (OLEDs),[1,8-10] and bioimaging and biosensing.[11] In addition, the strong ligand field strength of Ir(III) pushes the deactivating d-d state to a higher energy level and thus generates a long-lived lowest triplet excited state (*i.e.* the T_1 state) in Ir(III) complexes. This is a desirable feature for photosensitizers that have potential applications in energy upconversion[12,13] and photodynamic therapy.[14-16] By selecting appropriate ligands, Ir(III) complexes can absorb strongly in the visible spectral region, making them promising in photocatalysis.[17,18]

In addition to the well-studied emission properties and absorption of Ir(III) complexes targeting the aforementioned applications, reverse saturable absorption (RSA, a nonlinear absorption phenomenon in which the absorptivity of the materials increases with increased incident fluence due to a stronger excited-state absorption than the ground-state absorption) of Ir(III) complexes is another attractive feature associated with the efficient

[a] *Department of Chemistry and Biochemistry, North Dakota State University, Fargo, ND 58108-6050, USA. E-mail: Wenfang.Sun@ndsu.edu*
[b] *Hubei Collaborative Innovation Center for Advanced Organochemical Materials & Ministry of Education Key Laboratory for the Synthesis and Application of Organic Functional Molecules, Hubei University, Wuhan, 430062, P. R. China*
[c] *Key Laboratory of Eco-textiles, Ministry of Education, Jiangnan University, Wuxi 214122, P. R. China*
[d] *Materials and Nanotechnology Program, North Dakota State University, Fargo, ND 58108-6050, USA*
‡ These two authors contributed equally to this project.
Electronic Supplementary Information (ESI) available: Comparison of the experimental and calculated absorption spectra, solvent-dependent UV-vis absorption and emission spectra, time-resolved transient absorption spectra, and natural transition orbitals. See DOI: 10.1039/x0xx00000x

intersystem crossing induced by the heavy Ir metal and their broad and strong excited-state absorption,[19] which has potential applications in optical switching,[20] laser mode locking,[21] optical pulse shaping,[22] spatial light modulation,[23] and laser beam compression and limiting,[24,25] etc. Compared to the reported various inorganic,[26-28] organic,[29-34] or polymeric[35] RSA materials, Ir(III) complexes have the advantages of excellent chemical and photostability, facile tuning of the ground-state and excited-state absorption and T_1 state lifetime, and high quantum yield for triplet excited-state formation. Thus, they have drawn our and other groups' interest in exploring them as RSA materials.[19,36-51]

To develop ideal reverse saturable absorbers for broadband spectral and temporal optical limiting applications, the materials are required to possess long-lived, broad, and strong excited-state absorption but weak ground-state absorption in the visible to the near-infrared (NIR) regions in order to have large ratios of absorption cross sections between the excited and ground states (σ_{ex}/σ_0). However, it has remained to be a challenge to extend the ground-state absorption to the NIR regions while maintaining a long excited-state lifetime and strong excited-state absorption because a low-lying excited state promotes nonradiative decay processes to shorten the excited-state lifetime. Although it is possible to red shift the ground-state absorption of organic molecules while keeping a long-lived T_1 state, such a red-shift typically requires an extended π-conjugation or a large degree of charge transfer in the molecule. These features would induce very large ground-state absorption in the visible spectral region, causing a deep color of the molecule and reducing the linear transmission. Meanwhile, the significant ground-state absorption would dramatically decrease the σ_{ex}/σ_0 values and prevent the occurrence of RSA. Both of them are adverse features for optical limiting applications. On the contrary, by selecting appropriate π-conjugated ligands it is possible for Ir(III) complexes to have a weakly absorbing spin-forbidden ^{3}CT (charge transfer) / $^3\pi,\pi^*$ absorption band at 500 - 800 nm while still keeping a reasonably long-lived ligand-localized $^3\pi,\pi^*$ state.[19,43,46,50,51]

In seeking for solutions to address the aforementioned dilemma in developing broadband reverse saturable absorbers, we have studied the photophysics and RSA of a variety of monocationic Ir(III) complexes with different degrees of π-conjugation or substituents on the diimine (N^N) and/or cyclometalating (C^N) ligands.[19,36-51] Our studies revealed that the T_1 state lifetime was dramatically increased upon extending π-conjugation of the N^N ligand via incorporating π-conjugated substituents to this ligand owing to more N^N ligand-centered $^3\pi,\pi^*$/^{3}ILCT (intraligand charge transfer) characters being introduced to the T_1 state.[36,44,50] However, this approach had a minor impact on the energy of the lowest-energy absorption band. In contrast, expanding π-conjugation of the N^N ligand via benzannulation at the appropriate sites of this ligand induced a bathochromic shift of the lowest-energy absorption band but reduced the T_1 lifetime.[37,38,52] By combining these two approaches, it is possible to obtain Ir(III) complexes with weak, red-shifted low-energy absorption band and relatively long-lived T_1 state.[50] These studies demonstrated the feasibility and promise of employing Ir(III) complexes as broadband reverse saturable absorbers and the feasibility of modulating the RSA of the Ir(III) complexes via ligand structural modifications. However, the T_1 lifetimes of the complexes obtained with these characters were still limited to tens of nanoseconds.[50]

To solve this problem, in this work, we synthesized two new Ir(III) complexes bearing 6,6′-bis(7-benzothiazolylfluoren-2-yl)-2,2′-biquinoline ligand (structures shown in Scheme 1), aiming to improve the T_1 lifetime and the triplet excited-state absorption of the resultant Ir(III) complexes while red-shifting the low-energy absorption band. 2,2'-Biquinoline was chosen as the N^N ligand because our previously studied Ir(III) complexes bearing this ligand possessed a spin-forbidden ground-state absorption band at 500-650 nm.[37,41] 7-Benzothiazolylfluoren-2-yl was selected as the π-conjugated substituent because incorporating this substituent to the N^N ligands of Ir(III) complexes could induce broad and intense excited-state absorption in the visible to the NIR regions and resulted in strong optical limiting at 532 nm.[36,44,50] In our new complexes, 7-benzothiazolylfluoren-2-yl motifs were connected to 2,2′-biquinoline ligand by single or triplet bonds to extend and vary the degree of π-conjugation of the N^N ligand, and 1-phenylisoquinoline was chosen as the C^N ligand. The UV-vis absorption, emission and transient absorption were investigated to understand the impact of extended π-conjugation on the photophysics of the complexes. Time-dependent density functional theory (TDDFT) calculations were carried out to unambiguously ascribe the nature of the optical transitions. Nonlinear transmission measurements were conducted to demonstrate the RSA of the complexes for nanosecond laser pulses at 532 nm.

Experimental section

Synthesis and characterization

All reagents were purchased from Aldrich or Alfa Aesar and used as received unless otherwise stated. Compounds **1**,[41] **2**,[44] **3**,[45,46] and **4**[47] were synthesized following the literature procedures. Tetrahydrofuran (THF) and triethylamine (Et_3N) were dehydrated over sodium benzophenone ketyl under N_2 and then distilled. Silica gels (230–400 mesh) used for chromatography were purchased from Alfa Aesar. **L-1**, **L-2**, **Ir-1**, and **Ir-2** were characterized via ^{1}H NMR, HRMS, and elemental analyses. ^{1}H NMR spectra were recorded on a Varian Oxford-500 or Oxford-400 VNMR spectrometer. ESI-HRMS analyses were performed on a Bruker BioTOF III mass spectrometer. Elemental analyses were conducted by NuMega Resonance Laboratories, Inc. in San Diego, California. The synthetic details and characterization data for **L-1**, **L-2**, **Ir-1**, and **Ir-2** are provided below.

Ligand L-1. A stirred mixture of **1** (80 mg, 0.193 mmol), **2** (277 mg, 0.425 mmol), K_2CO_3 (3.4 g, 24.6 mmol), $Pd(PPh_3)_4$ (45 mg, 0.039 mmol), toluene (25 mL), and H_2O (10 mL) was purged with nitrogen and heated to reflux for 30 h. The mixture was cooled to rt, poured into water, and extracted with ethyl acetate. The organic layer was combined and dried over anhydrous Na_2SO_4 and the solvent was removed. The residue was purified by column chromatography on Al_2O_3 gel (hexane/ethyl acetate = 50/1 - 20/1, v/v) to give **L-1** as a yellow solid (120 mg, yield: 48%). ^{1}H NMR (500 MHz, $CDCl_3$): δ 8.96 (d, J=8.5 Hz, 2H), 8.44 (d, J=8.5 Hz, 2H), 8.37 (d, J=8.5 Hz, 2H), 8.22-8.09 (m, 10H), 7.98-7.77 (m, 10H), 7.53 (t, J=7.5 Hz, 2H), 7.41 (t,

J=7.5 Hz, 2H), 2.29-2.13 (m, 8H), 1.05-0.50 (m, 60H). ESI-HRMS: m/z Calcd for $[C_{90}H_{98}N_4S_2]^+$, 1300.7344; found, 1300.7390. Anal. Calcd (%) for $C_{90}H_{98}N_4S_2$: C, 83.16; H, 7.60; N, 4.31. Found: C, 83.40; H, 8.00; N, 3.93.

Ligand L-2. A stirred mixture of **1** (80 mg, 0.193 mmol), **4** (233 mg, 0.425 mmol), PPh_3 (21 mg, 0.078 mmol), $Pd(PPh_3)_2Cl_2$ (28 mg, 0.039 mmol) and CuI (8 mg, 0.039 mmol) in Et_3N (10 mL) and THF (20 mL) was purged with nitrogen and heated to 80 °C under nitrogen for 24 h. The mixture was cooled to rt and the solvent was removed. The residue was washed with brine and extracted with CH_2Cl_2. The organic layer was combined and dried over anhydrous Na_2SO_4 and the solvent was removed. The residue was purified by column chromatography on Al_2O_3 gel (hexane/ethyl acetate = 50/1 - 20/1, v/v) to give **L-2** as a yellow solid (120 mg, yield: 46%). ^{1}H NMR (500 MHz, $CDCl_3$): δ 8.91 (d, *J*=8.5 Hz, 2H), 8.34 (d, *J*=9.0 Hz, 2H), 8.23 (d, *J*=8.5 Hz, 2H), 8.20-8.08 (m, 8H), 7.97-7.90 (m, 4H), 7.84 (d, *J*=8.0 Hz, 2H), 7.80 (d, *J*=7.5 Hz, 2H), 7.69-7.61 (m, 4H), 7.53 (t, *J*=7.5 Hz, 2H), 7.41 (t, *J*=7.5 Hz, 2H), 2.26-2.20 (m, 8H), 1.05-0.50 (m, 60H). ESI-HRMS: m/z Calcd for $[C_{94}H_{98}N_4S_2]^+$, 1348.7344; found: 1348.7327. Anal. Calcd (%) for $C_{94}H_{98}N_4S_2 \cdot 0.2CH_2Cl_2 \cdot 2.0C_6H_{14}$: C, 82.97; H, 8.29; N, 3.64. Found: C, 82.81; H, 8.48; N, 3.83.

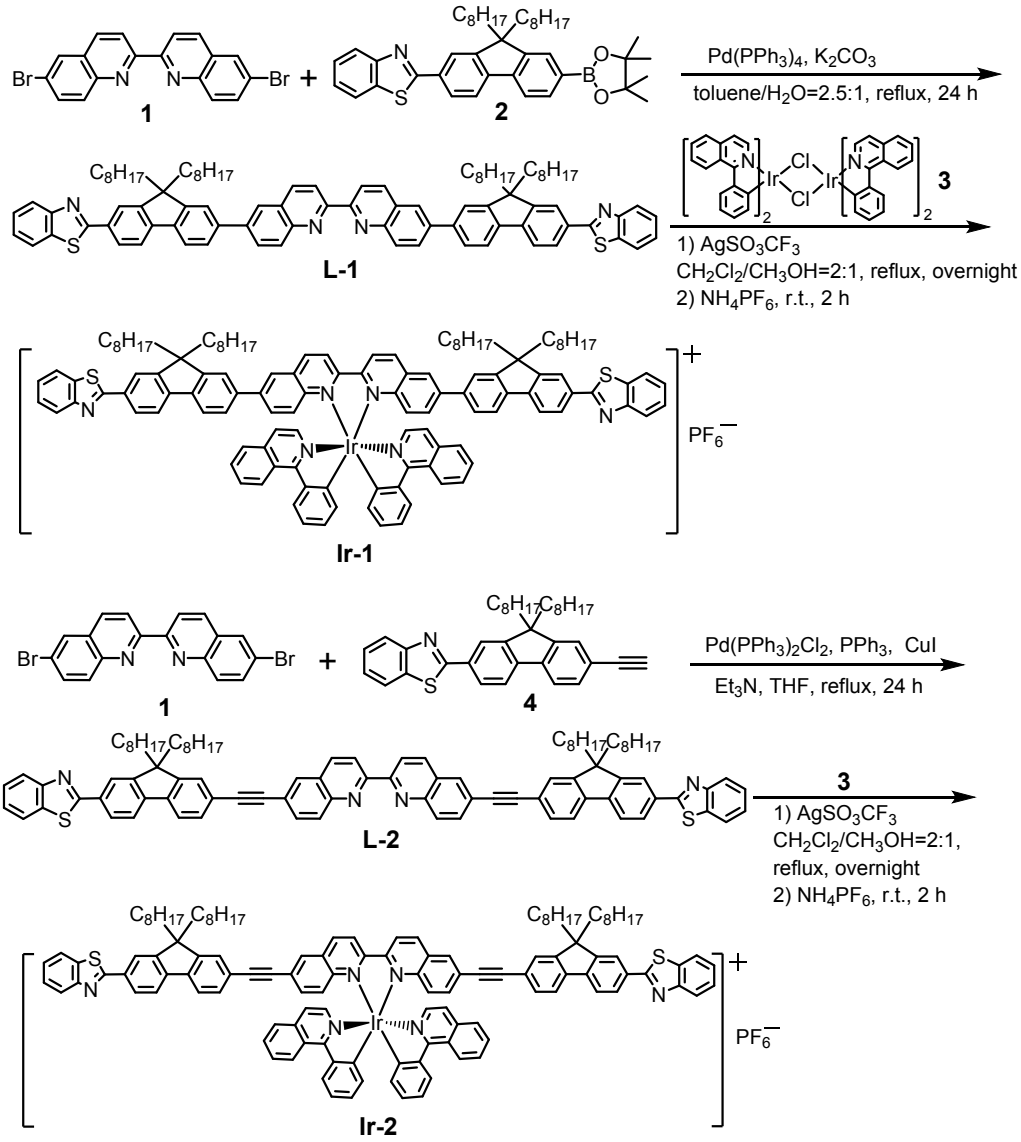

Scheme 1 Structures and synthetic route for ligands **L-1** and **L-2**, and complexes **Ir-1** and **Ir-2.**

Complex Ir-1. Compounds **L-1** (70 mg, 0.054 mmol), **3** (38 mg, 0.030 mmol) and $AgSO_3CF_3$ (15 mg, 0.054 mmol) were added to degassed CH_2Cl_2/MeOH (30 mL, 2/1, v/v) and the mixture was refluxed overnight under nitrogen. After cooling to rt, 10-fold NH_4PF_6 was added. The suspension was stirred at rt for 2 h and then filtered to remove any insoluble salts. After removal of the solvent, the crude product was purified by column chromatography on silica gel (CH_2Cl_2/ethyl acetate = 50/1, v/v) to afford **Ir-1** as a brownish-green solid (50 mg, yield: 80%). ^{1}H NMR (500 MHz, $CDCl_3$): δ 8.88 (dd, *J*=8.5, 16 Hz, 4H), 8.75 (d, *J*=8.0 Hz,

2H), 8.27 (d, *J*=6.5 Hz, 2H), 8.20-8.05 (m, 8H), 7.97-7.70 (m, 16H), 7.65-7.57 (m, 4H), 7.52 (t, *J*=8.0 Hz, 2H), 7.45-7.38 (m, 4H), 7.33 (d, *J*=6.0 Hz, 2H), 7.19-7.10 (m, 2H), 6.97-6.90 (m, 2H), 6.52 (d, *J*=7.5 Hz, 2H), 2.22-2.05 (m, 8H), 1.02-0.45 (m, 60H). ESI-HRMS: m/z Calcd for $[C_{120}H_{118}IrN_6S_2]^+$, 1899.8501; found: 1899.8542. Anal. Calcd (%) for $C_{120}H_{118}F_6IrN_6PS_2 \cdot 0.5C_6H_{14}$: C, 70.73; H, 6.03; N, 4.02. Found: C, 70.37; H, 6.36; N, 4.19.

Complex Ir-2. Compounds **L-2** (60 mg, 0.0445 mmol), **3** (28.3 mg, 0.0223 mmol) and $AgSO_3CF_3$ (15 mg, 0.0445 mmol) were added to degassed CH_2Cl_2/MeOH (30 mL, 2/1, v/v) and the mixture was refluxed overnight under nitrogen. After cooling to rt, 10-fold NH_4PF_6 was added. The suspension was stirred at rt for 2 h and then filtered to remove any insoluble salts. After removal of the solvent, the crude product was purified by column chromatography on silica gel (CH_2Cl_2/ethyl acetate = 50/1, v/v) to give **Ir-2** as a brownish-green solid (40 mg, yield: 68%). ^{1}H NMR (500 MHz, $CDCl_3$): δ 8.85 (d, *J*=8.5 Hz, 4H), 8.63 (d, *J*=8.5 Hz, 2H), 8.29-8.23 (m, 2H), 8.18-8.08 (m, 6H), 8.07-8.02 (m, 2H), 7.93 (d, *J*=8.0 Hz, 2H), 7.88 (d, , *J*=8.0 Hz, 2H), 7.84-7.74 (m, 10H), 7.71-7.65 (m, 2H), 7.60-7.49 (m, 6H), 7.40 (t, *J*=6.5 Hz, 2H), 7.32 (d, *J*=6.5 Hz, 2H), 7.25-7.20 (m, 2H), 7.15 (t, *J*=7.5 Hz, 2H), 6.93 (t, *J*=7.5 Hz, 2H), 6.48 (d, *J*=7.5 Hz, 2H), 2.20-2.01 (m, 8H), 1.00-0.48 (m, 60H). ESI-HRMS: m/z Calcd for $[C_{124}H_{118}IrN_6S_2]^+$, 1948.8524; found: 1948.8534. Anal. Calcd (%) for $C_{124}H_{118}F_6IrN_6PS_2 \cdot 4.4CHCl_3$: C, 58.89; H, 4.71; N, 3.21. Found: C, 58.74; H, 5.10; N, 3.40.

Photophysical measurements

Spectroscopic grade solvents purchased from VWR International were employed for the photophysical studies. A Shimadzu UV-2501 spectrophotometer was used to record the UV-vis absorption spectra, and a Jobin-Yvon FluoroMax-4 fluorometer / phosphorometer was used to measure the steady-state emission spectra. The emission quantum yields were determined by the relative actinometry method[53] in degassed solvents, in which a degassed acetonitrile solution of $[Ru(bpy)_3]Cl_2$ (Φ_{em} = 0.097, λ_{ex} = 436 nm)[54] was utilized as the reference for complexes **Ir-1** and **Ir-2**, and a 1 N sulfuric acid solution of quinine bisulfate (Φ_{em} = 0.546, λ_{ex} = 347.5 nm)[55] was used as the reference for ligands **L-1** and **L-2**. An Edinburgh LP920 laser flash photolysis spectrometer was employed for measuring the nanosecond transient absorption (TA) spectra, decays, and triplet lifetimes in argon-sparged (40 min) toluene solutions. The third harmonic output (355 nm) of a Nd:YAG laser (Quantel Brilliant, pulse duration = 4.1 ns; repetition rate = 1 Hz) was used as the excitation light for the TA measurements. The triplet excited-state absorption coefficients ($\varepsilon_{T1\text{-}Tn}$) at the TA band maxima were estimated by the singlet depletion method,[56] and the triplet excited state quantum yields were determined by the relative actinometry[57] with SiNc in benzene solution (ε_{590} = 70,000 L mol^{-1} cm^{-1}, Φ_T = 0.20)[58] as the reference.

Nonlinear transmission measurements

Nonlinear transmission experiment was carried out to demonstrate the reverse saturable absorption (RSA) of complexes **Ir-1** and **Ir-2** at 532 nm using a Quantel Brilliant laser (pulse width: 4.1 ns, repetition rate: 10 Hz) as the light source. Complexes **Ir-1** and **Ir-2** were dissolved in toluene and the concentrations of the sample solutions were adjusted to obtain a linear transmission of 80% at 532 nm in a 2-mm cuvette. The experimental details followed that reported by our group previously.[45] The radius of the beam waist at the focal point was approximately 96 μm using a 40-cm plano-convex lens.

Computational methods

All calculations were performed employing Gaussian09 software package.[59] Geometries of the ligands and Ir(III) complexes and their ground state electronic structures were obtained based on density functional theory (DFT) using the hybrid PBE0 functional[60] and mixed LANL2DZ/6-31G* basis set for Ir(III) ion and the remaining atoms, respectively. To capture the major relativistic effects on molecular structures, the nonlinear exchange and potential were estimated by decoupling the large components and small components of the Dirac Hamiltonian through unitary transformations with Douglas-Kroll-Hess approximation,[61] in which the electronic structure calculation was based on the upper diagonal part of the Hamiltonian.[62]

The absorption spectra and emission energies were calculated using linear response time-dependent DFT (TDDFT) by iteratively solving the eigenvalue equation based on Davidson algorithm[63-66] and utilizing the same LANL2DZ/6-31G* basis set and PBE0 functional as those used in the ground state calculations. The absorption spectral profiles were plotted implementing Gaussian line width broadening (~0.1 eV) to 40 optical transitions obtained from TDDFT calculations to represent inhomogeneous thermal broadening of experimental spectra. The emission energies were obtained by optimizing the lowest singlet excited-state geometry using analytical gradient TDDFT[67] for fluorescence and TDDFT for phosphorescence using the triplet ground-state geometry obtained from unrestricted DFT optimization (Δ-SCF approach).[68-70]

Conductor-like polarizable continuum model (CPCM)[71,72] was used in both DFT and TDDFT calculations as implemented in Gaussian09. Toluene was chosen as the solvent media for **L-1**, **L-2**, **Ir-1**, and **Ir-2** to be consistent with experimental data. Excited-state calculations were based on state-specific approach,[73] which accounted for the non-equilibrium effects of slow component of reaction field of a solvent.

The hole-electron pairs contributing to the optical transition were represented by natural transition orbital (NTO) analysis based on the unitary transformation of transition density matrix of a selected excited state.[74,75] The ground- and excited-state electronic densities were plotted by Chemcraft-1.7 software[76] setting isovalue as 0.02. The applied methodology, including the functional, basis set, solvent model, and NTO analysis, has been proven to be efficient and accurate enough for calculations of optical spectra of many other Ir(III) complexes.[19,36-38,40-47,50]

Results and discussion

Electronic absorption

The UV-vis absorption of **L-1**, **L-2**, **Ir-1**, and **Ir-2** was investigated in toluene with concentrations varying from 1×10^{-6} to 1×10^{-4} mol L^{-1}, and the absorption spectra (experimental and calculated) are displayed in Fig. 1. The absorption of both the ligands and the

complexes obeyed the Beer's law in the concentration range studied, implying the lack of ground-state aggregation in this range. The absorption band maxima and molar extinction coefficients are listed in Table 1. The simulated absorption spectra via TDDFT calculations matched well with the experimental spectra, as demonstrated in ESI Fig. S1.

As depicted in Fig. 1a, the absorption spectra of **L-1** and **L-2** in toluene possess intense absorption band(s) at 300−430 nm. Based on the large molar extinction coefficients of the absorption band(s), the minor solvatochromic effect (ESI Fig. S2), and the natural transition orbitals (NTOs) (Table 2), these bands predominantly arise from the $^1\pi,\pi^*$ transitions mixed with minor intramolecular charge transfer (^{1}ICT) character. The absorption spectrum of **L-2** possesses larger extinction coefficients and is red-shifted compared to that of **L-1**, which is in line with the extended π-conjugation via incorporating the C≡C triple bonds in **L-2**.

The absorption spectra of **Ir-1** and **Ir-2** (Fig. 1a) are composed of two major absorption bands: one intense structured band at 300-380 nm ($\varepsilon \approx 1.23$ - 1.46×10^5 L.mol^{-1}.cm^{-1}) and another broad, strong and featureless band at 380-520 nm ($\varepsilon \approx 7.0\times10^4$ L.mol^{-1}.cm^{-1}). In addition, a broad but weak absorption tail appears at 520-650 nm ($\varepsilon \leq 2.0\times10^3$ L.mol^{-1}.cm^{-1}). Considering the large molar extinction coefficients, the vibronically-resolved structures, the minor solvatochromic effect (ESI Fig. S2), and the NTOs (ESI Table S1) representing the major transitions contributing to the high-energy absorption bands at 300-380 nm, we attribute the parentage of these bands predominantly to the ligand-localized $^1\pi,\pi^*$ transitions, admixing with minor ^{1}MLCT/^{1}LLCT configurations at the high-energy side (300-310 nm). The broad and structureless band at 380-520 nm is indicative of a dominant charge-transfer transition, which is a characteristic band found in Ir(III) and Ru(II) complexes bearing fluorenyl-substituted diimine ligand.[19,36,40,41,44,77] In view of the NTOs corresponding to transitions contributing to this band (Table 2), this band is ascribed to the N^N ligand-localized intraligand charge transfer (^{1}ILCT) / $^1\pi,\pi^*$ transitions and mixed with ^{1}MLCT/^{1}LLCT configurations. Because of the large spin-orbit coupling constant of Ir, spin-forbidden transitions directly from the singlet ground state to the ^{3}MLCT/^{3}LLCT/$^3\pi,\pi^*$ triplet excited states are possible, which contribute to the tail at 520-650 nm. This characteristics is in accordance with that found in many other cationic Ir(III) complexes,[19,36-38,40-46,50-52] and the larger π-conjugation of the 2,2'-biquinoline ligand made this band red-shifted in comparison to those in complexes bearing the 2,2'-bipyridine or 1,10-phenanthroline ligands.[37]

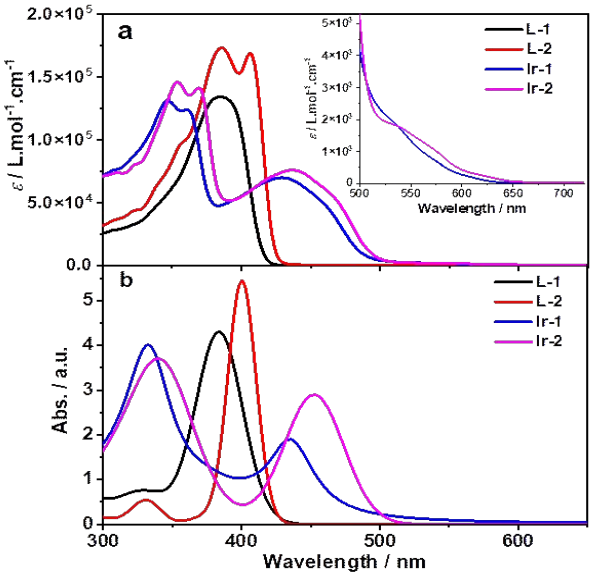

Fig. 1 (a) Experimental and (b) calculated absorption spectra of **L-1**, **L-2**, **Ir-1**, and **Ir-2** in toluene.

Comparison of the absorption spectra of **Ir-1** and **Ir-2** clearly reveals that incorporation of the C≡C triple bonds into the N^N ligand leads to a red-shift of all absorption bands in **Ir-2** with respect to those in **Ir-1**. This trend reflects the involvement of the substituted diimine ligand in the optically active transitions contributing to the major absorption bands in these two complexes.

Table 1 Electronic absorption, emission, and triplet excited-state absorption parameters of **L-1**, **L-2**, **Ir-1**, and **Ir-2** in toluene.

	λ_{abs}/nm (ε/10^4 L mol^{-1} cm^{-1})	λ_{em}/nm (τ_{em}/ns); Φ_{em}	$\lambda_{T1\text{-}Tn}$/nm (τ_T/ns; $\varepsilon_{T1\text{-}Tn}$/10^4 L mol^{-1} cm^{-1}); Φ_T
L-1	385 (13.40)	417 (–), 442 (–); 0.91	751 (19690; 8.89); 0.075
L-2	385 (17.29), 406 (16.84)	420 (–), 447 (–); 0.91	762 (58930; 3.23); 0.082
Ir-1	346 (13.11), 361 (12.33), 429 (6.98)	640 (800); 0.096	755 (790; 3.62), 536 (770; 4.46); 0.14
Ir-2	354 (14.58), 369 (14.08), 436 (7.59)	648 (350); 0.059	770 (330; 4.40), 554 (330; 5.10); 0.10

Table 2 Natural transition orbitals (NTOs) representing the lowest energy transitions for **L-1**, **L-2**, **Ir-1**, and **Ir-2** in toluene.

	States	Hole	Electron
L-1	S_1 383 nm f = 4.30	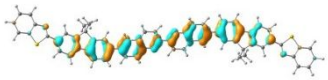 81%	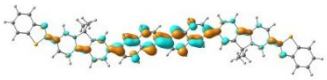 81%
		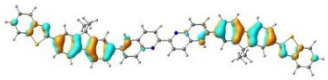 15%	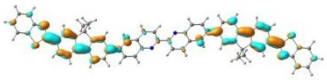 15%

	S_2 359 nm f = 0.001	59% 37%	59% 37%
L-2	S_1 400 nm f = 5.44	78% 16%	78% 16%
	S_2 371 nm f = 0.14	56% 37%	56% 37%
Ir-1	S_1 450 nm f = 0.05		
	S_2 435 nm f = 1.63		
Ir-2	S_1 453 nm f = 2.84		
	S_2 435 nm f = 0.07		
	S_3 413 nm f = 0.06		

Emission

The emission characteristics of **L-1**, **L-2**, **Ir-1**, and **Ir-2** were investigated in different solvents at room temperature. The normalized emission spectra in toluene are illustrated in Fig. 2, and the emission spectra in different solvents are given in ESI Fig. S3. The emission parameters are summarized in Tables 1 and 3.

Ligands **L-1** and **L-2** are highly emissive in all solvents used in our study. The small Stokes shifts compared to their respective absorption spectra and the short lifetimes (<10 ns and thus were unable to be measured on our instrument) indicate that they are fluorescence in nature. However, the parentage of the emitting states varied when the polarity of solvent changed. As shown in Fig. 2 and ESI Fig. S3, the fluorescence spectra of **L-1** and **L-2** in toluene and hexane are clearly vibronically resolved and thus the emission is ascribed to be from the $^1\pi,\pi^*/^1$ICT state. This attribution is supported by the NTOs of the emitting states for these two ligands calculated by analytical TDDFT in toluene (ESI Table S2). When the polarity of the solvent increased, the spectra lost some vibronic features and became broader in CH_2Cl_2 and acetone. In CH_3CN, the emission essentially became structureless and the fluorescence quantum yield decreased in comparison to those in less polar solvents (Table 3). These changes reflect the increased intramolecular charge transfer character when the polarity of the solvent increases. Similar to the trend observed in the UV-vis absorption spectra of **L-1** and **L-2**, the extended π-

conjugation in **L-2** induced a red-shift of the fluorescence spectra with respect to the spectra of **L-1** in each solvent.

The emission of complexes **Ir-1** and **Ir-2** appeared at 640-650 nm, which is dramatically red-shifted with respect to their excitation wavelengths and with reference to their corresponding ligands. The emission is prone to oxygen quenching and has a lifetime of hundreds of ns (Tables 1 and 3). These characteristics suggest phosphorescence in nature. As shown in Figs. 2 and S3, the emission spectra in toluene and hexane possess some vibronic structures, while the spectra become structureless and red-shifted when the polarity of solvent increases. Accompanied by this change, the emission lifetimes and quantum yields decrease with the increased solvent polarity. The vibronic structure, longer lifetime, and higher quantum yield of the emission in toluene, hexane, and CH_2Cl_2 imply that the phosphorescence in these solvents likely emanate from a ligand-centered $^3\pi,\pi^*$ state, possibly mixed with some charge transfer characters. This attribution is supported by the NTOs of the emitting T_1 state in toluene displayed in Table 4, which indicate a predominant N^N ligand-localized $^3\pi,\pi^*$ configuration with a minor contribution from the ^{3}MLCT/^{3}ILCT transitions. The prominent involvement of the N^N ligand in the emission induced lower emission energies for **Ir-2** in each corresponding solvent compared to those of **Ir-1** owing to the extended π-conjugation of the N^N ligand in **Ir-2**. In contrast to the emission spectra in these less polar solvents, the emission spectra of **Ir-1** and **Ir-2** in more polar solvents such as acetone and acetonitrile were structureless and red-shifted accompanied by shorter lifetimes and reduced quantum yields, suggesting an increased charge transfer contribution to the emitting state in the more polar solvents.

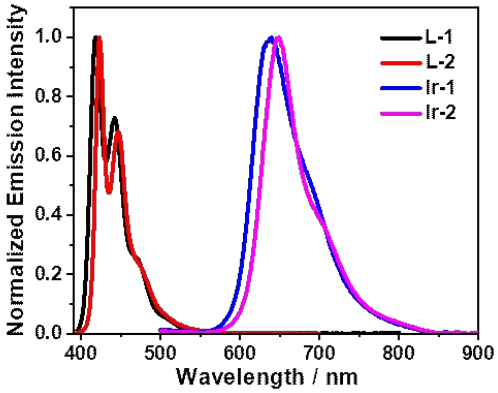

Fig. 2 Normalized emission spectra of **L-1**, **L-2**, **Ir-1**, and **Ir-2** in toluene. The excitation wavelength was 385 nm for **L-1** and **L-2**, 429 nm for **Ir-1**, and 436 nm for **Ir-2**.

Table 3 Emission parameters of **L-1**, **L-2**, **Ir-1**, and **Ir-2** in different solvents at room temperature

	λ_{em}/nm (τ_{em}/ns); Φ_{em}				
	Hexane[a]	Toluene	CH_2Cl_2	Acetone	CH_3CN
L-1	408 (–), 433 (–); 0.94	417 (–), 442 (–); 0.91	428 (–), 444 (–); 0.91	424 (–), 443 (–); 0.89	444 (–); 0.82
L-2	413 (–), 439 (–); 0.93	420 (–), 447 (–); 0.91	432 (–); 0.84	445 (–); 0.73	452 (–); 0.76
Ir-1	635 (950); 0.085	640 (800); 0.096	657 (920); 0.12	658 (580); 0.058	657 (650); 0.053
Ir-2	643 (540); 0.066	648 (350); 0.059	672 (490); 0.066	675 (190); 0.020	673 (180); 0.017

[a] With 15% toluene for **Ir-1** and **Ir-2.**

Table 4 NTOs corresponding to the phosphorescent emitting states of **Ir-1** and **Ir-2** in toluene.

	λ_{em} / nm	Electron	Hole
Ir-1	655		
Ir-2	665		

Transient absorption

In addition to phosphorescence discussed above, highly populated T_1 state can possibly give rise to excited-state absorption, which is another characteristic of the T_1 state. Investigation of the excited-state absorption will also aid in our deeper understanding of how the extended π-conjugation of the N^N ligand impacts on the triplet excited-state characteristics. Therefore, the nanosecond transient absorption (TA) of **L-1**, **L-2**, **Ir-1**, and **Ir-2** was studied in degassed toluene solutions. The TA spectra of **L-1**, **L-2**, **Ir-1**, and **Ir-2** at zero delay upon excitation at 355 nm are displayed in Fig. 3, and the excited-state absorption coefficients as well as the triplet lifetimes and quantum yields are summarized in Table 1. The time-resolved TA spectra of **L-1**, **L-2**, **Ir-1**, and **Ir-2** are presented in ESI Fig. S4.

Fig. 3 illustrates that ligands **L-1** and **L-2** possess very broad positive TA bands at 420–800 nm with similar spectral features. Bleaching occurred at 385 nm for **L-1**, and 383 nm and 408 nm for **L-2**, which are in line with the $^1\pi,\pi^*/^1$ICT absorption bands in their UV-vis absorption spectra. Because of the extended π-conjugation in **L-2**, its TA band maximum is slightly red-shifted with a slightly stronger intensity than that of **L-1**, accompanied by a much longer T_1 lifetime than that of **L-1**. In view of the very long triplet lifetimes, it is reasonable for us to assign the transient absorbing excited states of **L-1** and **L-2** to their $^3\pi,\pi^*$ states.

The positive TA bands of **Ir-1** and **Ir-2** appeared at 480-800 and 486-800 nm, with respective band maxima at 536/755 and

554/770 nm, respectively, indicating that the excited-state absorption is stronger than that of the ground state in these spectral regions for the two complexes. Bleaching occurred at 435 and 442 nm, respectively, which are coincident with the positions of the predominant ^{1}ILCT/$^1\pi,\pi^*$ absorption bands in their respective UV-vis spectra. The triplet lifetimes of **Ir-1** and **Ir-2** deduced from the decays of their TA signals are in line with those obtained from the decays of emission signals, implying the transient absorbing excited state being the emitting excited state, *i.e.* the $^3\pi,\pi^*$/^{3}MLCT/^{3}ILCT states. Similar to the trend observed in their UV-vis absorption and emission spectra, expanding the π-conjugation of the N^N ligand led to a red-shift of the positive TA bands and the bleaching band in **Ir-2** with a reduced T_1 lifetime compared to those for **Ir-1**.

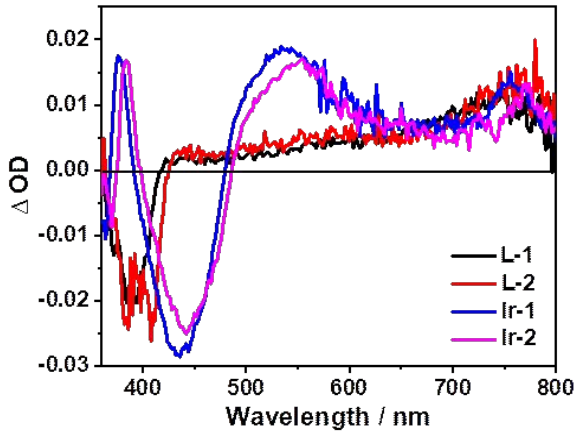

Fig. 3 Nanosecond TA spectra of **L-1**, **L-2**, **Ir-1**, and **Ir-2** in toluene at zero delay after excitation at 355 nm. A_{355} = 0.4 in a 1-cm cuvette.

Reverse saturable absorption (RSA)

As mentioned in the Introduction section, RSA occurs when the excited-state absorption is stronger than the ground-state absorption. Complexes **Ir-1** and **Ir-2** exhibited stronger excited-state absorption than ground-state absorption in the regions of 490-800 nm, suggesting that they potentially display RSA in this spectral region. To demonstrate the RSA, nonlinear transmission experiments were conducted for complexes **Ir-1** and **Ir-2** in toluene solutions at 532 nm using a 4.1-ns pulsed laser with the linear transmission of all solutions adjusted to be 80% at 532 nm in a 2-mm cuvette, and the linear transmission *vs*. incident energy curves for complexes **Ir-1** and **Ir-2** are shown in Figure 4. The transmission of **Ir-1** and **Ir-2** decreased drastically with the increased incident energy, testifying the occurrence of RSA. The strength of the RSA for **Ir-2** is slightly stronger than that of **Ir-1**, suggesting that extending π-conjugation of the N^N ligand in **Ir-2** enhanced the RSA. To justify the observed RSA trend, the ratio of the excited-state absorption cross section (σ_{ex}) to that of the ground state (σ_0) that was revealed to be the key parameter determining the strength of RSA was estimated according to the method reported by us previously.[27] Briefly, the σ values were obtained from the ε values at 532 nm according to the conversion equation $\sigma = 2303\varepsilon/N_A$ (where N_A is the Avogadro's constant), where the ε values were deduced from the UV-vis absorption spectra and the transient absorption spectra for ε_0 and ε_{ex}, respectively. The resultant σ_0 and σ_{ex} values along with the σ_{ex}/σ_0 ratios are listed in Table 5. **Ir-1** and **Ir-2** possess very similar σ_0 values at 532 nm, but the σ_{ex} value of **Ir-2** is slightly larger than that of **Ir-1**, resulting in the slightly larger σ_{ex}/σ_0 ratio for **Ir-2**, which correlates well with the observed RSA trend.

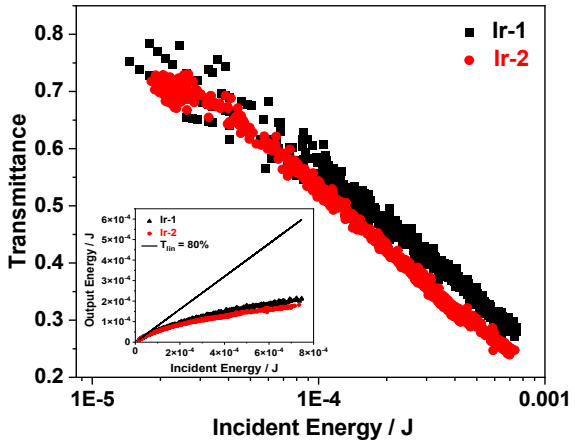

Fig. 4 Nonlinear transmission curves of **Ir-1** and **Ir-2** in toluene for 4.1 ns laser pulses at 532 nm in a 2 mm cuvette. For each sample, the linear transmission was adjusted to 80%. The radius of the beam waist at the focal plane was approximately 96 μm. The inset shows the corresponding output energy vs. incident energy curves for these two complexes.

Table 5 Ground-state and excited-state absorption cross sections of **Ir-1** and **Ir-2** in toluene at 532 nm.

	Ir-1	Ir-2
$\sigma_0/10^{-18}$ cm^2	8.2	8.1
$\sigma_{ex}/10^{-18}$ cm^2	168	183
σ_{ex}/σ_0	20.5	22.6

Conclusions

Two heteroleptic cationic Ir(III) complexes bearing 7-benzothiazolylfluoren-2-yl substituted 2,2'-biquinoline ligand via single or triplet bond linkage were synthesized and investigated to understand the effects of extending the π-conjugation of the diimine ligand on their photophysics and reverse saturable absorption. Our studies revealed that extending π-conjugation of the diimine ligand red-shifted the ground-state absorption, emission, and transient absorption bands in **Ir-2**. The extended π-conjugation of the diimine ligand also switched the T_1 state to predominantly the diimine ligand localized $^3\pi,\pi^*$ state, resulting in a relatively long-lived T_1 state while the energy of the T_1 state was reduced. The stronger excited-state absorption than that of the ground-state of **Ir-1** and **Ir-2** gave rise to a dramatic RSA, with a slightly stronger RSA for **Ir-2** than for **Ir-1**, which correlated well with their σ_{ex}/σ_0 ratios. The broad but weak ground-state

absorption at 500-650 nm, the much stronger triplet excited-state absorption in the same spectral region, accompanied by the relatively long T_1 lifetime made these complexes promising candidates as broadband reverse saturable absorbers. Although the broadband optical limiting was not demonstrated in this work due to the limitation of our instrument, our studies on the ground-state and excited-state absorption have shed light on the potential of these complexes as broadband optical limiting materials. The strategy used in this work could also be applied to other transition-metal complexes for broadband optical limiting application.

Conflicts of interest

There are no conflicts to declare.

Acknowledgements

The authors are grateful to National Science Foundation (DMR-1411086) for support.

Notes and references

1 H. Xu, R. Chen, Q. Sun, W. Lai, Q. Su, W. Huang and X. Liu, *Chem. Soc. Rev*., 2014, **43**, 3259−3302.

2 I. M. Dixon, J.–P. Collin, J.–P. Sauvage, L. Flamigni, S. Encinas and F. Barigelletti, *Chem. Soc. Rev.*, 2000, **29**, 385−391.

3 S. Lamansky, P. Djurovich, D. Murphy, F. Abdel–Razzaq, R. Kwong, I. Tsyba, M. Bortz, M. Mui, R. Bau and M. E. Thompson, *Inorg. Chem.,* 2001, **40**, 1704−1711.

4 J. I. Goldsmith, W. R. Hudson, M. S. Lowry, T. H. Anderson and S. Bernhard, *J. Am. Chem. Soc*., 2005, **127**, 7502−7510.

5 E. Holder, B. M. W. Langeveld and U. S. Schubert, *Adv. Mater.,* 2005, **17**, 1109−1121.

6 M. Mydlak, C. Bizzarri, D. Hartmann, W. Sarfert, G. Schmid and L. De Cola, *Adv. Funct. Mater.,* 2010, **20**, 1812−1820.

7 C. D. Sunesh, G. Mathai and Y. Choe, *ACS Appl. Mater. Interfaces,* 2014, **6**, 17416−17425.

8 K. Mullen and U.Scherf, Organic Light−Emitting Devices; Wiley−VCH: Weinheim, Germany, 2006.

9 H.−T. Mao, C.−X. Zang, G.−G. Shan, H.−Z. Sun, W.−F. Xie and Z.−M. Su, *Inorg. Chem.,* 2017, **56**, 9979−9987.

10 Y.Wang, S. M. Wang, J. Q. Ding, L. X. Wang, X. B. Jing and F. S. Wang, *Chem. Commun.,* 2017, **53**, 180−183.

11 Y. Chen, R. Guan, C. Zhang, J. Huang, L. Ji and H. Chao, *Coord. Chem. Rev.,* 2016, **310**, 16−40.

12 J. Sun, F. Zhong, X. Yi and J. Zhao, *Inorg. Chem.,* 2013, **52**, 6299−6310.

13 L. Ma, S. Guo, J. Sun, C. Zhang, J. Zhao and H. Guo, *Dalton Trans.,* 2013, **42**, 6478−6488.

14 O. J. Stacey and S. J. A. Pope, *RSC Adv.,* 2013, **3**, 25550−25564.

15 D. Maggioni, M. Galli, L. D'Alfonso, D. Inverso, M. V. Dozzi, L. Sironi, M. Iannacone, M. Collini, P. Ferruti, E. Ranucci and G. D'Alfonso, *Inorg. Chem.,* 2015, **54**, 544−553.

16 L. K. McKenzie, I. V. Sazanovich, E. Baggaley, M. Bonneau, V. Guerchais, J. A. G. Williams, J. A. Weinstein and H. E. Bryant, *Chem. Eur. J.,* 2017, **23**, 234−238.

17 H. Huo, X. Shen, C. Wang, L. Zhang, P. Rose, L.−A. Chen, K. Harms, M. Marsch, G. Hilt and E. Meggers, *Nature,* 2014, **515**, 100−103.

18 H. Huo, C. Wang, K. Harms and E. Meggers, *J. Am. Chem. Soc.,* 2015, **137**, 9551−9554.

19 L. Wang, P. Cui, S. Kilina and W. Sun, *J. Phys. Chem. C,* 2017, **121**, 5719−5730.

20 C. Li, L. Zhang, R. Wang, Y. Song and Y. Wang, *J. Opt. Soc. Am. B,* 1994, **11**, 1356−1360.

21 A. Penzkofer, *Appl. Phys. B,* 1988, **46**, 43−60.

22 K. P. J. Reddy, *Curr. Sci.,* 1991, **61**, 520−526.

23 S. Speiser and M. Orenstein, *Appl. Opt.,* 1988, **27**, 2944−2948.

24 Y. B. Band, D. J. Harter and R. Bavli, *Chem. Phys. Lett.,* 1986, **126**, 280−284.

25 J. W. Perry, D. Alvarez, I. Choong, K. Mansour, S. R. Marder and K. J. Perry, *Opt. Lett.,* 1994, **19**, 625−627.

26 U. Gurudas, E. Brooks, D. M. Bubb, S. Heiroth, T. Lippert and A. Wokaun, *J. Appl. Phys.*, 2008, **104**, 073107.

27 J.-J. Wu, Y.-R. Tao, J.-N. Wang, Z.-Y. Wu, L. Fan and X.-C. Wu, *Nanoscale*, 2016, **8**, 10371-10379.

28 L. W. Tutt and S. W. McCahon, *Opt. Lett.*, 1990, **15**, 700-702.

29 J. W. Perry, K. Mansour, S. R. Marder, K. J. Perry, D. Alvarez and I. Choong, *Opt. Lett.*, 1994, **19**, 625-627.

30 N. K. M. N. Srinivas, S. V. Rao and D. N. Rao, *J. Opt. Soc. Am. B*, 2003, **20**, 2470-2479.

31 L. W. Tutt and A. Kost, *Nature*, 1992, **356**, 225-226.

32 R. C. Hoffman, K. A. Stetyick, R. S. Potember and D. G. McLean, *J. Opt. Soc. Am. B*, 1989, **6**, 772-777.

33 W. Blau, H. Byrne, W. M. Dennis and J. M. Kelly, *Opt. Commun.*, 1985, **56**, 25-29.

34 S. Hughes, G. Spruce, B. S. Wherrett, K. R. Welford and A. D. Lloyd, *Opt. Commun.*, 1993, **100**, 113-117.

35 K. A. Vishnumurthy, M. S. Sunitha and A. Adhikari, *Eur. Polymer J.*, 2012, **48**, 1575-1585.

36 Y. Li, N. Dandu, R. Liu, Z. Li, S. Kilina and W. Sun, *J. Phys. Chem. C*, 2014, **118**, 6372−6384.

37 R. Liu, N. Dandu, J. Chen, Y. Li, Z. Li, S. Liu, C. Wang, S. Kilina, B. Kohler and W. Sun, *J. Phys. Chem. C,* 2014, **118**, 23233−23246.

38 W. Sun, C. Pei, T. Lu, P. Cui, Z. Li, C. McCleese, Y. Fang, S. Kilina, Y. Song and C. Burda, *J. Mater. Chem. C,* 2016, **4**, 5059−5072.

39 T. M. Pritchett, M. J. Ferry, W. M. Shensky, A. G. Mott, D. J. Stewart, S. L. Long, J. E. Haley, Z. Li and W. Sun, *Opt. Lett.,* 2015, **40**, 186-189.

40 C. Pei, P. Cui, C. McCleese, S. Kilina, C. Burda and W.Sun, *Dalton Trans.,* 2015, **44**, 2176–2190.

41 X. Zhu, L. Lystrom, L. S. Kilina and W. Sun, *Inorg. Chem.,* 2016, **55**, 11908–11919.

42 X. Zhu, P. Cui, S. Kilina, W. Sun, *Inorg. Chem.,* 2017, **56**, 13715–13731.

43 B. Liu, L. Lystrom, S. Kilina and W. Sun, *Inorg. Chem.,* 2019, **58**, 476−488.

44 Y. Li, N. Dandu, R. Liu, L. Hu, S. Kilina and W. Sun, *ACS Appl. Mater. Interfaces,* 2013, **5**, 6556–6570.

45 Z. Li, P. Cui, C. Wang, S. Kilina and W. Sun, *J. Phys. Chem. C,* 2014, **118**, 28764−28775.

46 C. Wang, L. Lystrom, H. Yin, M. Hetu, S. Kilina, S. A. McFarland and W. Sun, *Dalton Trans*., 2016, **45**, 16366–16378.
47 Z. Li, H. Li, B. J. Gifford, W. D. N. Peiris, S. Kilina and W. Sun, *RSC Adv.,* 2016, **6**, 41214–41228.
48 K.-Y. Kim, R. T. Farley and K. S. Schanze, *J. Phys. Chem. B,* 2006, **110**, 17302 −17304.
49 H. Zhao, P. V. Simpson, A. Barlow, G. J. Moxey, M. Morshedi, N. Roy, R. Philip, C. Zhang, M. P. Cifuentes and M. G. Humphrey, *Chem. Eur. J.,* 2015, **21**, 11843–11854.
50 H. Li, S. Liu, L. Lystrom, S. Kilina and W. Sun, *J. Photochem. Photobiol. A,* 2020, **400**, 112609.
51 B. Liu, L. Lystrom, S. L. Brown, E. K. Hobbie, S. Kilina and W. Sun, *Inorg. Chem.*, 2019, **58**, 5483-5493.
52 Q. Zhao, S. Liu, M. Shi, C. Wang, M. Yu, L. Li, F. Li, T. Yi and C. Huang, *Inorg. Chem*., 2006, **45**, 6152-6160.
53 J. N. Demas and G. A. Crosby, Review. *J. Phys. Chem.,* 1971, **75**, 991–1024.
54 K. Suzuki, A. Kobayashi, S. Kaneko, K. Takehira, T. Yoshihara, H. Ishida, Y. Shiina, S. Oishi and S. Tobita, *Phys. Chem. Chem. Phys.,* 2009, **11**, 9850–9860.
55 D. F. Eaton, *Pure Appl. Chem.,* 1988, **60**, 1107–1114.
56 I. Carmichael and G. L. Hug, *J. Phys. Chem. Ref. Data,* 1986, **15**, 1–250.
57 C. V. Kumar, L. Kumar and P. K. Das, *J. Chem. Soc., Faraday Trans. 2,* 1984, **80**, 783–793.
58 P. A. Firey, W. E. Firey, J. R. Firey, M. E. Kenney and M. A. Rodgers, *J. Am. Chem. Soc.,* 1988, **110**, 7626–7630.
59 E. van Lenthe, E.-J. Baerends and J. G. Snijders, *J. Chem. Phys.,* 1994, **101**, 9783–9792.
60 J. P. Perdew, K. Burke and M. Ernzerhof, *Phys. Rev. Lett.,* 1996, **77**, 3865–3868.
61 J. E. Peralta and G. E. Scuseria, *J. Chem. Phys.,* 2004, **120**, 5875–5881.
62 A. Wolf, M. Reiher and B. A. Hess, *J. Chem. Phys.,* 2002, **117**, 9215–9226.
63 M. E. Casida, *Recent advances in density functional methods,* 1995, **1**, 155–192.
64 L. Künne, *Z. Phys. Chem.,* 1998, **204**, 263–264.
65 R. Bauernschmitt and R. Ahlrichs, *Chem. Phys. Lett.,* 1996, **256**, 454–464.
66 E. R. Davidson, *J. Comput. Phys.,* 1975, **17**, 87–94.
67 S. Van Gisbergen, J. Snijders and E. Baerends, *Comput. Phys. Commun.,* 1999, **118**, 119–138.
68 S. Kilina, D. Kilin, and S. Tretiak. *Chem. Rev.,* 2015, **15**, 5929–5978.
69 V. Albert, E. Badaeva, S. Kilina, M. Sykora and S. Tretiak. *J. Lumines.,* 2011, **131**, 1739-1746.
70 E. Badaeva, V. Albert, S. Kilina, A. Koposov, M. Sykora and S. Tretiak. *Phys. Chem. Chem. Phys.,* 2010, **12**, 8902-8913.
71 V. Barone and M. Cossi. *J. Phys. Chem. A,* 1998, **102**, 1995–2001.
72 M. Cossi, N. Rega, G. Scalmani and V. Barone. *J. Comput. Chem.,* 2003, **24**, 669–681.
73 R. Cammi, S. Corni, B. Mennucci and J. Tomasi. *J. Chem. Phys.,* 2005, **122**, 104513.
74 R. L. Martin. *J. Chem. Phys.,* 2003, **118**, 4775–4777.
75 E. R. Batista and R. L. Martin. *Encyclo. Comput. Chem.,* 2004.
76 G. Zhurko and D. Zhurko. *ChemCraft,* 2009, version 1.6, Build.
77 L. Wang, H. Yin, M. A. Jabed, M. Hetu, S. Monro, C. Wang, S. Kilina, S. A. McFarland and W. Sun. *Inorg. Chem.,* 2017, **56**, 3245-3259.

ARTICLE